Inorganic Chemistry Communications 149 (2023) 110446

Contents lists available at ScienceDirect

Inorganic Chemistry Communications

journal homepage: www.elsevier.com/locate/inoche

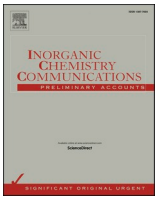

Short communication

# Improving mechanical, biological, and adhesive properties of synthesized mineral trioxide aggregate by adding chitosan

Mariyam Mariyam [a,c], Siti Sunarintyas [b], Nuryono Nuryono [a,*]

[a] Department of Chemistry, Faculty of Mathematics and Natural Sciences, Universitas Gadjah Mada, Sekip Utara, Yogyakarta 55281, Indonesia
[b] Department of dental Biomaterial, Faculty of Dentistry, Universitas Gadjah Mada, Sekip Utara Yogyakarta 55281, Indonesia
[c] Department of Chemistry, Institut Teknologi Sumatera, Terusan Ryacudu, Jati Agung, Lampung 35365, Indonesia

ARTICLE INFO

*Keywords:*
Mineral trioxide aggregate
Calcium silicate
Chitosan
Sol-gel

ABSTRACT

In this study, chitosan (with various concentrations) was added to modify the synthesized white mineral trioxide aggregate (WMTA). WMTA was prepared through the sol–gel method at a low-temperature heating (1000 °C). The component of WMTA was 60 % CaO, 20 % $SiO_2$, 2 % $Al_2O_3$, and 18 % $Bi_2O_3$, and the product was characterized using TG/DTA, FTIR, XRD, and SEM instrumentations. The characterization results showed similar characteristics of the synthesized WMTA compared to the commercial one (Pro Root). In further work, we studied the effect of chitosan addition on the characteristics of hydrated WMTA. The results showed that modification with chitosan led to enhancing the antibacterial, mechanical, and adhesive properties of WMTA. WMTA modified with 4 wt% of chitosan resulted in the highest diametral tensile and compressive strength on day 7 and exhibited the most intimate adhesive interface with dentin. The loss mass percentage of all groups (less than 3 %) and radiopaque values exceeding 3 mm Al met the requirement as a dental material, except for WMTA with 6 wt% chitosan. All WMTAs generated alkaline conditions by releasing $Ca^{2+}$ ions in an artificial saliva solution, which was beneficial for antibacterial and biocompatibility. WMTA modified with 4 wt% chitosan provided the best mechanical, biological, and adhesive properties, so further investigation is necessary for an in-vivo study.

## 1. Introduction

Deep caries tooth may lead to pulp exposure and advance to root canal injury. This damage should be treated through root canal treatment [1]. One of the root canal filling materials commonly used is white mineral trioxide aggregate (WMTA) which is notably a hydrophilic synthetic powder. MTA consists of tricalcium silicate ($C_3S$), dicalcium silicate ($C_2S$), tricalcium aluminate ($C_3A$), and radiopacity agent. MTA has been extensively used for root fracture repair, root-end induction, apexification, pulp capping, and root-end filling material [2,3].

The synthesis of WMTA is usually performed by a solid-state method, which is time-consuming and has high energy spent (calcination temperature approximately 1200 °C to 1500 °C) [4]. In this study, we applied a sol–gel method followed by calcination at 1000 °C, which is a lower temperature than in previous investigations [4,5]. The sol–gel method has been widely used to synthesize various compounds such as ceramics, nanostructures and composites [6–9]. This technique is one of the simplest ways to obtain a high-quality product with controlled size and texture, and highly pure and homogenous particles [10]. Compared to the solid-state method, which gives non-homogeneity of the reaction, the sol–gel method will lead to ultrafine and homogenous particles formation to improve its properties and effectiveness, specifically for enhancing mechanical characteristics in the early stages of the hydration reaction. These advantages have made it a popular technique for synthesizing various ceramic compounds, including MTA synthesis.

Although WMTA is an excellent dental material with its favorable biocompatibility, low sealing ability, porosity formation during hydration, and long setting time remain to be resolved [3,11,12]. These limitations may cause microleakage formation, low cement material strength, and the emergence of bacterial colonization in root canals, potentially leading to undesired inflammatory reactions [11,13]. Hence, it is essential to develop the characteristics of WMTA by modifying it with other materials to increase its adhesive, antibacterial and mechanical properties.

Many attempts have been proceeded to improve the physicochemical properties of WMTA while preserving its appropriate characteristics.

* Corresponding author.
*E-mail address:* nuryono_mipa@ugm.ac.id (N. Nuryono).

https://doi.org/10.1016/j.inoche.2023.110446
Received 25 September 2022; Received in revised form 16 January 2023; Accepted 20 January 2023
Available online 25 January 2023

Adding reinforcement materials such as polyvinyl alcohol, methylcellulose, and propylene glycol to WMTA remains insufficient to fulfill the requirement of standard dental materials [14–16]. Among several polymers, chitosan (poly-β-1,4-glucosamine) is a natural biopolymer with good biocompatibility, antibacterial activity, mucoadhesive and non-toxic properties [17]. Chitosan has been broadly used as a restorative material to repair hard tissues such as bones and teeth due to its capacity to induce mineralization [18]. Using chitosan in composite materials may reduce setting time and increase the bonding between the dentinal wall and the WMTA material by forming a tag-like structure [19,20]. The amino and hydroxyl groups may crosslink with other reactive molecules in collagen fiber to improve the bonding stability of the dentin-material interface by forming micro and nano-fibrillar tissues in protein molecules [19]. However, the study of chitosan/WMTA composite as a root canal treatment material has not been reported.

The present paper reports a study on the effect of chitosan on the properties of hydrated WMTA. The study includes the mechanical (diametral tensile and compressive strength) properties, radiopacity, mass loss percentage, pH, $Ca^{2+}$ release, antibacterial activity, and an adhesive interface between the dentinal wall and WMTA.

## 2. Experimental

### 2.1. Synthesis of white mineral trioxide aggregate

The analytical grade materials, including calcium carbonate ($CaCO_3$) (*Merck p.a*), tetraethylorthosilicate (TEOS) (*Merck p.a*), aluminum nitrate hydrate ($Al_2(NO_3)_3{\cdot}9H_2O$) (*Merck p.a*), and bismuth oxide ($Bi_2O_3$) (*Merck p.a*) were used for the synthesis of WMTA. WMTA containing CaO, $SiO_2$, $Al_2O_3$, and $Bi_2O_3$ of 60 %, 20 %, 18 % and 2 % respectively, were synthesized using the sol–gel method [8,21]. A 200 μL base catalyst (ammonia solution 25 %, purchased from *Merck EMSURE® ISO,Reag. Ph Eur*) was added to 200 mL of deionized water and stirred for 5 min. TEOS (6.93 mL) as a silica source was poured into the ammonia solution under stirring for 10 min. $CaCO_3$ (10.71 g) and $Al_2(NO_3)_3{\cdot}9H_2O$ (0.70 g) were dispersed to the solution sequentially at 80 °C and stirred until a homogeneous mixture was obtained. Stirring and heating were continued at 120 °C to accelerate water evaporation to get a white viscous gel of WMTA. The gel was dried in an oven at 100 °C for 1 h to yield solid gel. Part of the gel was subjected to TG/DTA analysis (*Exstar 7300 series*), and the rest was heated in a furnace at 1000 °C for 3 h. The white powder obtained (8.0 g) was then mixed with 1.76 g $Bi_2O_3$ (18 % w/w) and sieved through a 200 mesh to obtain un-hydrated WMTA. The resulting material was characterized with XRD (*PANalytical X'Pert3 Powder in the range of 5°-60° for 2θ with radiation of Cu-Kα (40 kV, 30 mA)*), FTIR spectrophotometer (*8201PC Shimadzu*), and Scanning Electron Microscope (*JSM-6510OLA*).

### 2.2. Effect of chitosan on hydrated WMTA properties

Chitosan (high mol. wt. *Sigma-Aldrich*) was added to the synthesized WMTA in the hydration process. The hydration was performed by mixing 1 g WMTA with 0.5 mL of liquid (the composition is presented in Table 1). The ratio of powder (in gram) to liquid (in mL) for hydration was 2:1, following the procedure recommended for the hydration of commercial WMTA (C-WMTA). After a certain hydration period, the mechanical properties, radiopacity, pH, $Ca^{2+}$ ion release, mass loss percentage, WMTA-dentin interface, and antibacterial activity were determined and evaluated.

### 2.3. Mechanical properties test

Mechanical property tests included diametral tensile and compressive strength evaluation. The test proceeded according to ISO 9917. Each hydrated sample (n = 3 per group) was molded to a cylinder shape (6 mm in height and 4 mm in diameter for the compression test; 3 mm in height and 4 mm in diameter for a tensile test). The parameter measurements of all groups were performed after 7 days of hydration. Each specimen was placed at a Universal testing Machine (UTM) with test loading at 0.01 N force and 10 mm/min test speed. The maximum load needed to break the samples was recorded as a mechanical test value.

### 2.4. Radiopacity test

The radiopacity test was carried out following ISO 6876; 9971–1 and ANSI/ADA (n = 3 per group). Samples were hydrated and molded to a thin cylindrical shape (1 mm in height and 5 mm in diameter) in a clear plastic mold. All specimens were left at room temperature for 24 h. Then the samples were placed next to an aluminum step wedge and irradiated with a 7 mA X-ray at 70 kV. The distance between the specimens and the X-ray source was 30 cm with 0.2 s of exposure time. The radiopaque value was quantified by comparing the aluminum step wedge thickness that is calculated with Equation (1).

$$A = -log(1 - \frac{G}{255}) \quad (1)$$

Where A is the absorbance value, and G is the grayscale value of the aluminum stepwedge digital image.

### 2.5. Percentage of mass loss, pH, and $Ca^{2+}$ ion Release.

All hydrated samples were molded in a cylindrical shape with dimensions of 3 mm in height and 4 mm in diameter (n = 3 per group). The mass loss test was carried out according to ISO 6876. After setting, each specimen was weighed and denoted as initial mass. Each specimen was immersed in an artificial saliva solution. The solution was collected and renewed after 1, 7, and 14 days. Before and after immersion on predefined days, all specimens were weighed to determine the mass loss percentage of the sample. The pH value was measured on a saturated solution with a pH meter (*SevenCompact™ Mettler Toledo*), while $Ca^{2+}$ ion release was quantified using Atomic Absorption Spectrometer (*ContrAA 300 Analytic Jena*).

### 2.6. WMTA-Dentin interface evaluation

The WMTA-dentin bonding interface was evaluated qualitatively by performing JSM-6510OLA Scanning Electron Microscope. Human premolar teeth were used (n = 3 per group) and perforated in a cylindrical cavity (2 mm in diameter, 3 mm in height) with one end open. All teeth were washed in distilled water and let dry in the oven. Each sample was loaded into the cavity without any packing pressure and stored at 37 °C for 7 days. The specimens were then sectioned horizontally using a low-speed saw and immersed in artificial saliva to remove any fine particles. The specimens were vacuumed to remove any residual water before further analysis. WMTA-dentin adhesive interfaces were observed on the exposed surface of the dentin with 1000x magnification.

### 2.7. Antibacterial activity test

Antibacterial activity tests were carried out against *Enterococcus faecalis* (ATCC 29212) and *Pseudomonas aeruginosa* (ATCC 10145) by using the agar diffusion method. Agar media were prepared by stirring 1.30 g of Nutrient Broth (NB) in 100 mL of distilled water. Agar of 2 % (w/w) was put into the NB solution and heated under stirring. Autoclave sterilizations were performed at 120 °C under 1 atm pressure for 30 min. The media were poured into the petri dish and let harden. Bacterial cultures were inoculated into sterile distilled water and homogenized by using a vortex. 100 μL of the bacterial solution was poured into the media, and each sample was placed in a different petri dish. Chloramphenicol was used as the positive control, and distilled water as the negative control. Petri dishes were tightly sealed and placed in the incubator for 24 h at 37 °C. The biological activity was determined by

the inhibition zone formed.

## 3. Results and discussion

### 3.1. Characterization of WMTA

**TG/DTA**. The mass change of WMTA gel during the calcination can be quantified by TG/DTA (Fig. 1). The TG/DTA was operated from 27 to 1200 °C with an increasing temperature of 5 °C per minute. The first mass loss at 100–200 °C occurred as the release of water molecules trapped in the sample. The further mass loss of 9.4 % at the temperature of 526 °C was due to the release of water molecules bound to $Ca(OH)_2$, an endothermic process as observed in the DTA profile diagram [4,22]. The second mass loss of 42 % is due to the $CaCO_3$ decomposition generating CaO moiety, which initiates the formation of new phases in WMTA at 700–750 °C. This decomposition occurred through the endothermic process, as presented in Eq. (2).

$$CaCO_3(s) \rightarrow CaO(s) + CO_2(g) \quad (2)$$

The main trioxides (CaO, $SiO_2$, and $Al_2O_3$) of the synthesized WMTA can be aggregated to form $C_3S$, $C_2S$, and $C_3A$ through the high-temperature heating process. Calcium aluminate begins to form at the temperature range between 550 and 600 °C, which is depicted in the DTA curve as an exothermic peak and continues to transform to $C_3A$ above 700 °C [22,23]. The DTA curve shows the exothermic peak above 1000 °C, which is attributed to the formation of calcium silicate phases. This solid-state reaction is regarded starting with the intergranular contact of CaO and $SiO_2$ of the cement material to form a fine and homogeneous aggregate with several factors influenced [22]. The linear curve above 800 °C does not show any further mass loss. $C_3S$, $C_2S$, and $C_3A$ formations in the WMTA synthesis were influenced by the temperature and duration of heating used in the calcination process [4,20]. The synthesis of WMTA is mainly carried out at the high-temperature treatment of 1100–1300 °C [4,8,21], which is a nongreen synthesis. We successfully applied the sol–gel method followed by 1000 °C heating temperature to synthesize WMTA, a lower temperature used than in prior studies. The use of 1000 °C heating temperature in the synthesis of WMTA is based on the Terner diagram that the calcium silicate phase formation starts above 900 °C.

**XRD Analysis.** The XRD diffraction pattern of the synthesized WMTA reveals new phases formed, which are identified as $C_3S$, $C_2S$, and $C_3A$. These new phases formed are due to the thermal treatment on the dry gel of WMTA according to the results of the TG/DTA. The diffraction pattern (Fig. 2.) depicts characteristic peaks of $C_3S$ (JCPDS 00–042-0551) at $2\theta = 29°$, and 34°, $C_2S$ (JCPDS 00–031-0299) around $2\theta = 50$ – 54°, $C_3A$ (JCPDS 00–032-0150) is detected at $2\theta = 37°$ while $Bi_2O_3$ (JCPDS 00–050-1088) is identified at $2\theta = 25$ – 35°. However, overlapping peaks between $C_3S$ and $C_2S$ may occur since these two components have closed characteristics of 2θ angles around 32 – 41°. The intensity of $C_3S$ in WMTA may increase as the heating duration and temperature increase [4]. The difference between the C-WMTA and WMTA diffraction patterns is the appearance of the Portlandite peak at $2\theta = 18°$ observed in WMTA. The presence of Portlandite is due to the incomplete reaction of CaO and $SiO_2$ at 1000 °C, resulting in free lime at the end of the product. The heating temperature above 1300–1500 °C may lead to the completion of calcium silicate formation [24]. However, the presence of $Ca(OH)_2$ in WMTA can induce the formation of apatite layers through the release of $Ca^{2+}$ ions and react with body fluids [25].

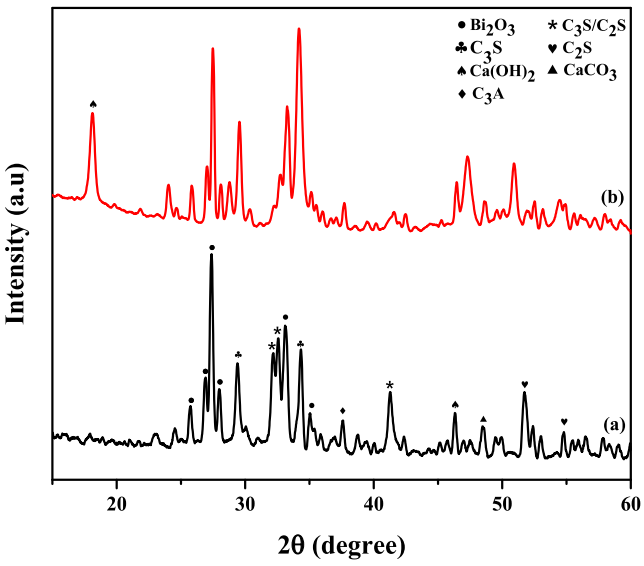


**Fig. 2.** XRD analysis of un-hydrated (a) C-WMTA and (b) WMTA.

**FTIR Analysis.** The WMTA functional groups were characterized using a *Shimadzu prestige 21 Fourier Transform Infrared Spectrophotometer* with a range of 300–4000 $cm^{-1}$ in wavelength. The result of FTIR spectra is consistent with those provided in the XRD data. The spectra (shown in Fig. 3) between C-WMTA and WMTA are in good agreement, which detects the successful synthesis of WMTA indicated by the specific bands of Si-O-Ca in $C_3S$ and $C_2S$. The sharp absorption band

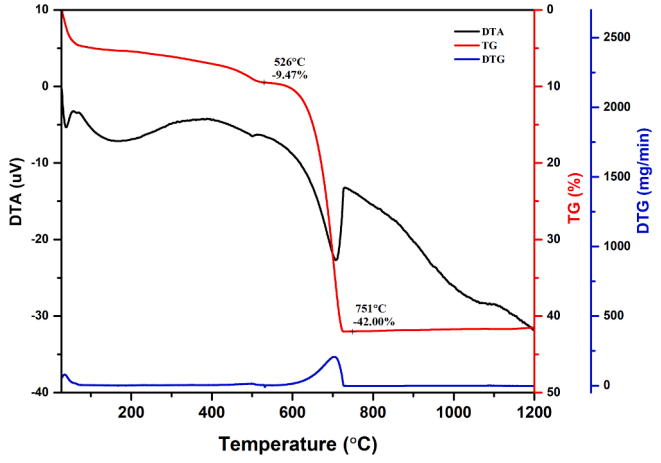


**Fig. 1.** TG/DTA curve of WMTA gel.

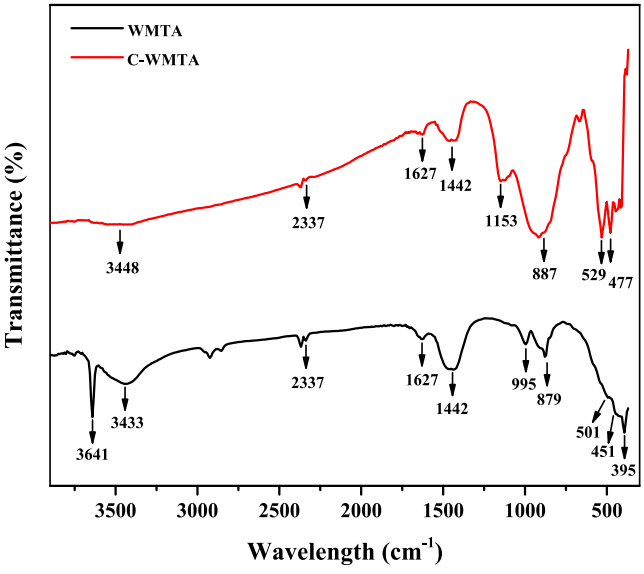


**Fig. 3.** FTIR spectra of C-WMTA and WMTA.

at 3641 cm-1 is identified as the O—H stretching vibration of $Ca(OH)_2$ contained in WMTA [8]. The characteristic of the O—H stretching vibration band from the $H_2O$ molecule is recognized with the broad signals at 3448 and 3433 $cm^{-1}$ corresponding to C-WMTA and WMTA, respectively [26]. The spectrum at 2337 $cm^{-1}$ is defined as the bending vibration of Si-O from the Si-O-Si (siloxane) linkage [27]. The stretching vibration of C—O in the carbonyl group of C-WMTA and WMTA is detected in a weak signal at 1627 $cm^{-1}$. Moreover, the band around 1442 $cm^{-1}$ is indicated as the asymmetric stretching vibration of the $CO_3^{2-}$ group [28].

The absorption band around 1153 $cm^{-1}$ is attributed to $SO_4^{2-}$ stretching mode from $CaSO_4$ anhydrite in C-WMTA, which verifies the presence of gypsum [29]. Calcium silicate phases are identified at the absorption band around 900–800 $cm^{-1}$ [4,8]. The overlapping absorption band of $C_3S$ and $C_2S$ is shown at 995 $cm^{-1}$ designated to WMTA [21]. The main vibration band of $C_3S$ symmetric stretching is depicted at 887 and 879 $cm^{-1}$ in C-WMTA and WMTA, respectively [30]. Siloxane groups in the silicate chain were also identified as Si–O–Si bending vibration at 477 $cm^{-1}$ and 451 $cm^{-1}$ for C-WMTA and WMTA, respectively [31–33]. $Bi_2O_3$ contained in both cement materials is identified in an absorption band at less than 600 $cm^{-1}$, seemingly superimposed with the silica absorption band [8]. Most of the main absorption bands contained in Pro Root are similar to WMTA, thus it can be said that the synthesis has been successful.

**SEM Analysis**. The surface morphology of C-WMTA and WMTA was analyzed by SEM image. The morphology of WMTA (as seen in Fig. 4) is observed as a non-uniform shape of particles. Agglomeration occurs in low temperature (1000 °C) heating treatment. Tiny cubic crystals are found in the SEM image, identified as unreacted $CaCO_3$ calcite in WMTA by the characteristic of its cubical appearance. Physically addition of 18 % (w/w) $Bi_2O_3$ to the WMTA (after calcination) shows the intertwined of $Bi_2O_3$ particles on the cement material. The content of $Bi_2O_3$ in WMTA may establish interconnected microchannels with a micropores system used to form crystal phases and the hydration process [34]. Most morphological grain forms of WMTA are visually similar to C-WMTA with inhomogeneous particle size.

### 3.2. Properties of WMTA/Chitosan composite

The hydration process of WMTA was carried out by mixing the powder with the liquid phase by a ratio of 2:1 (composition presented in Table 1.). FTIR analysis of hydrated WMTA was conducted after 7 days of hydration, and the IR spectra are presented in Fig. 5. The absorption band at 3641 $cm^{-1}$ is assigned to O—H stretching vibration of $Ca(OH)_2$ in hydrated WMTA, WMTA/Ch0, WMTA/Ch2, WMTA/Ch4, and WMTA/Ch6. The broadband of around 3448 $cm^{-1}$ detected in all WMTAs is designated as the presence of $H_2O$. The absorption band around 1400 $cm^{-1}$ is indicated the presence of $CO_3^{2-}$ groups in the samples [28]. The hydrated C-WMTA shows one specific band at 1118 $cm^{-1}$, indicating the presence of gypsum [29].

**Table 1**
Composition of hydrated WMTA.

| Sample Code | Liquid For Hydration |
|---|---|
| C-WMTA | Double distilled water |
| WMTA | Double distilled water |
| WMTA/Ch0 | 1 % acetic acid solution |
| WMTA/Ch2 | 2 % chitosan in 1 % acetic acid solution |
| WMTA/Ch4 | 4 % chitosan in 1 % acetic acid solution |
| WMTA/Ch6 | 6 % chitosan in 1 % acetic acid solution |

The shifted vibration band to a lower wavelength from 1000 $cm^{-1}$ to 900 $cm^{-1}$, and 890 to 870 $cm^{-1}$, detected the interaction of the silicate chain with the hydroxyl group of chitosan [20]. From the FTIR spectra, it can be seen the decrease in the intensity of $Ca(OH)_2$ (Fig. 5 c, d, e, and f) due to the reduction of Portlandite's solubility in the acid environment hence retards the hydration reaction of the cement. The addition of chitosan is another influence on a hydration reaction. Chitosan may cover the surface of the un-hydrated WMTA and prevent cement particles from contacting water while hindering Portlandite from dissolving in water [35].

SEM images of hydrated WMTAs (after 7 days of hydration time) are represented in Fig. 6. The CSH were identified as irregular grains in shape in all WMTAs. The calcium silicate hydrate (CSH), as the first product formed by the hydration process, may interact with other polymers in CSH interlayers. SEM images (Fig. 6. a, b) exhibit the presence of pores in hydrated WMTA microstructures (shown by yellow arrows). These pores will affect the mechanical properties of the cement, i.e., decreasing the compressive strength value, as presented in Table 2. On the other hand, adding chitosan in WMTA (Fig. 6. c, d, e) reveals dense structures of CSH and homogeneity at the surface area. Although it is difficult to quantify the grain size of CSH, the grain size is reduced when the chitosan is added, along with the improvement of their mechanical properties (Table 2). A change in the CSH morphology indicates that chitosan can act as a modifier to WMTA cement [36]. Chitosan-like gel fiber fills the space of the CSH region, and its adhesive properties can tighten the system between aggregates (shown by the red arrow in Fig. 6. c, d, e).

Some CSH particles are deposited on the chitosan gel, assuming that the interaction of polymer and silicate chain in the CSH interlayer occurs (as illustrated in Fig. 7). The protonation of free amino groups in chitosan occurs in acidic conditions and stabilizes when the system's pH is alkaline. This condition leads chitosan to form a gel, thus reducing the formation of the pores in hydrated WMTA. Previous studies revealed that Van Der Waals's interaction mainly contributed to the interaction between polymers and cement matrix [37].

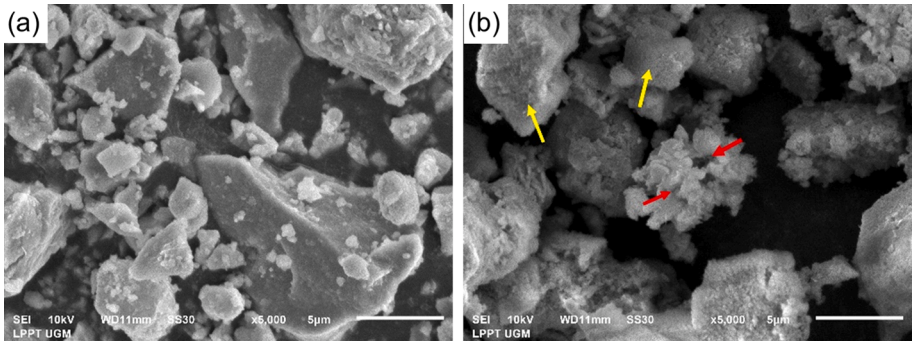


**Fig. 4.** SEM images of (a) C-WMTA and (b) WMTA (with 5000x magnification). The yellow arrow shows the presence of unreacted calcite in WMTA identified by the form of a cubic shape. The red arrow exhibited the presence of microchannels in WMTA utilized for the progression of the hydration reaction. (For interpretation of the references to colour in this figure legend, the reader is referred to the web version of this article.)

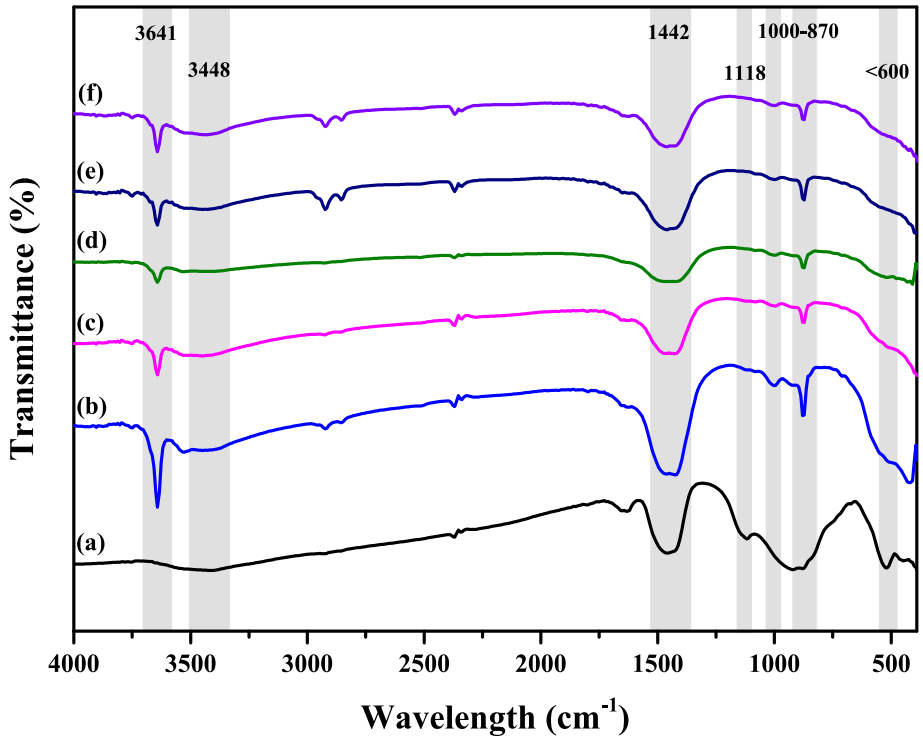


**Fig. 5.** FTIR spectra of hydrated (a) C-WMTA; (b) WMTA; (c) WMTA/Ch0; (d) WMTA/Ch2; (e) WMTA/Ch4; (f) WMTA/Ch6.

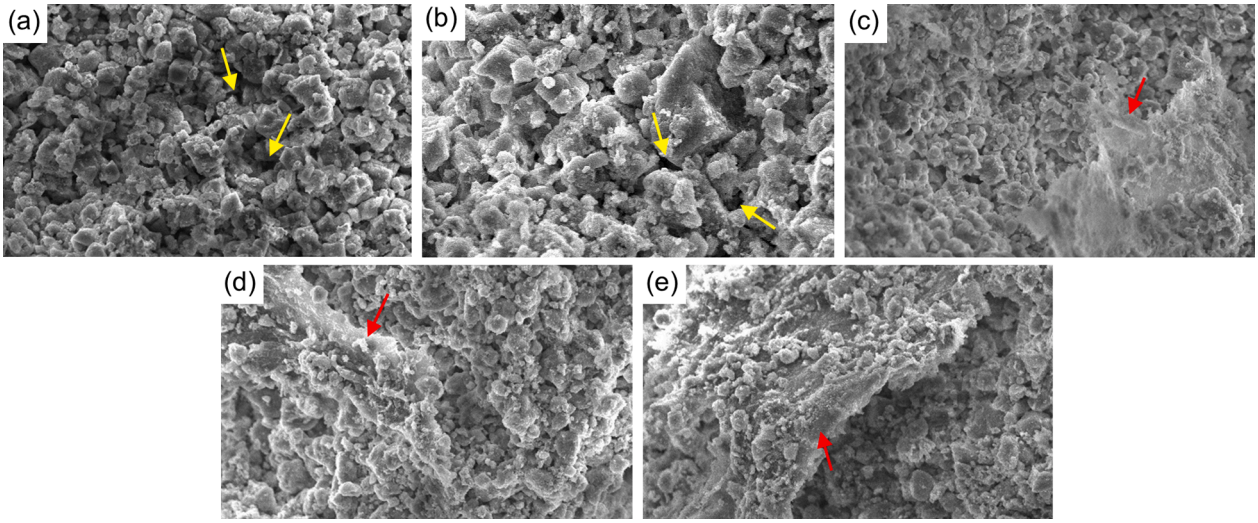


**Fig. 6.** SEM images of hydrated (a) WMTA; (b) WMTA/Ch0; (c) WMTA/Ch2; (d) WMTA/Ch4; (e) WMTA/Ch6 (with 1000x magnification). Yellow arrows show the presence of pores in WMTA, and red arrows depict the chitosan-like fiber gel that fills the space of the CSH system. (For interpretation of the references to colour in this figure legend, the reader is referred to the web version of this article.)

**Table 2**
Mechanical property (MPa) of tested groups.

| Sample Code | Compressive Strength 7 Days | Diametral Tensile Strength 7 Days |
|---|---|---|
| C-WMTA | 4.70 ± 1.71 | 3.71 ± 0.01 |
| WMTA | 4.20 ± 0.65 | 3.11 ± 1.63 |
| WMTA/Ch0 | 4.01 ± 0.64 | 3.18 ± 0.80 |
| WMTA/Ch2 | 4.33 ± 0.57 | 3.67 ± 2.63 |
| WMTA/Ch4 | 5.40 ± 0.45 | 3.74 ± 0.00 |
| WMTA/Ch6 | 3.78 ± 0.65 | 2.82 ± 2.27 |

### *3.2.1. Mechanical property test*

The mechanical properties have been tested for diametral tensile and compressive strength according to ISO 9917. Adding an acidic solution instead of water to the WMTA reveals no significant effect on its mechanical properties. Thus it can be expected that the chitosan additives merely influence the improvement of compressive and tensile strength. The effect of chitosan on the compressive strength of WMTA is presented in Table 2, which reveals the improvement of compressive strength by adding 2 wt% and 4 wt% chitosan compared to chitosan-free WMTA. The highest compressive test value on day 7 is attributed to the WMTA/Ch4 compared to all samples. The result reveals that 4 wt% of chitosan additive to WMTA gives optimum composition for the mechanical test,

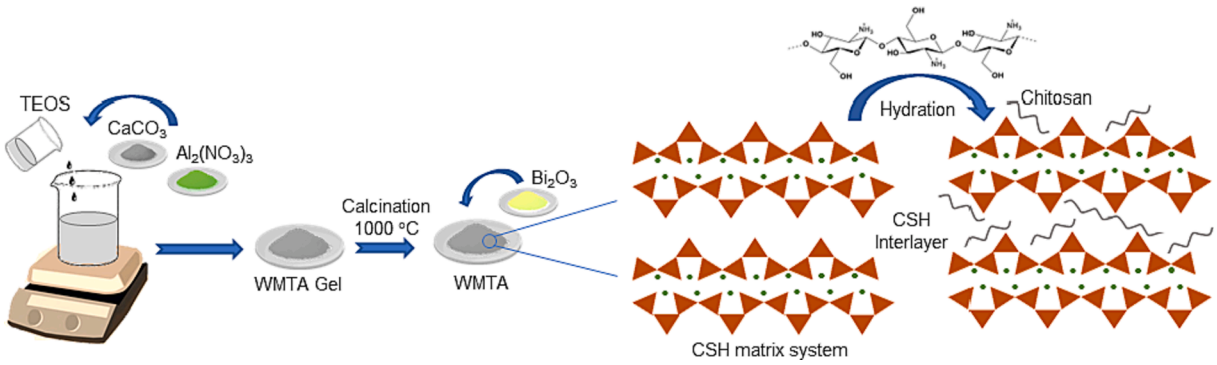


**Fig. 7.** Schematic of modified white mineral trioxide aggregate with chitosan.

showing the higher value of the compressive test on day 7.

This enhancement correlates with the role of chitosan as a reinforcement polymer to decrease porosity and strengthen the interaction between aggregates in the composites [35]. As seen in SEM images (Fig. 5) that the polymer is assumed to be intercalated in CSH interlayers and further forms hydrogen bonding between the –OH active group in the chitosan molecule and the silanol (-Si-OH) group in the silicate chain of the CSH region [37,38]. This intercalation and interaction may reduce the empty space and the thickness zone of adjacent CSH interlayers, hence improving the mechanical strength of WMTA/Chitosan composites [35]. Generally, chitosan has low to moderate mechanical properties [20], therefore adding considerable chitosan to WMTA may decrease the compressive strength of the cement material experienced in WMTA/Ch6. The highest diametral tensile strength value is addressed to WMTA/Ch4 compared to all tested groups. The addition of chitosan is investigated to enhance the adhesion between the cement matrix and the chitosan and improve the cement plasticity [36].

### 3.2.2. Radiopacity

The radiopacity test was done by comparing samples with the Aluminum step wedge under X-ray exposure. This test was intended to ease in distinguishing visibility between teeth and WMTA material when dental treatment is undertaken in the radiograph. According to iSO-6876:2012, WMTAs must have an adequate radiopacity value equivalent to 3 mm Al. Fig. 8. shows that each specimen has radiopaque properties equal to aluminum stepwedge thickness of 1–14 mm. Digital evaluation of the radiopacity value is calculated using Eq.1 using *ImageJ* software.

Of all the tested groups, C-WMTA possesses the highest radiopacity value (6.07), similar to previous research [39]. Table 3 shows no significant difference in radiopacity value between WMTA and WMTA/Ch0 due to the same bismuth oxide content in the specimens. The radiopacity values decrease gradually with the addition of chitosan due to the absence of radiopacifying properties in chitosan material [35]. However, the radiopacity values of all groups are above 3 mm Al, which defines that all experimented WMTAs qualify for the requirement of standard dental material recommended by ANSI/ADA.

### 3.2.3. Percentage of mass Loss, pH, and $Ca^{2+}$ ion release

The percentage of mass loss, pH, and $Ca^{2+}$ ion release was investigated in all group experiments. The mass loss test is intended to measure the number of mass losses when WMTA material is applied in the root canal. The partially washed-out WMTA may advance to microleakage and lead to bacterial colonization. Hence, the mass loss property plays an important part in determining the appropriate WMTA material. The

**Table 3**
Mass loss of tested groups.

| Time Intervals | Mass Loss (%) C-WMTA | WMTA | WMTA/Ch0 | WMTA/Ch2 | WMTA/Ch4 | WMTA/Ch6 |
|---|---|---|---|---|---|---|
| 1 Day | 2.69 ± 1.90 | 1.96 ± 1.38 | 2.12 ± 0.31 | 2.70 ± 1.38 | 0.68 ± 1.13 | 5.52 ± 1.96 |
| 7 Days | 1.37 ± 0.15 | 0.67 ± 1.13 | 1.52 ± 0.61 | 2.22 ± 1.13 | 1.37 ± 1.13 | 0.00 ± 0.00 |

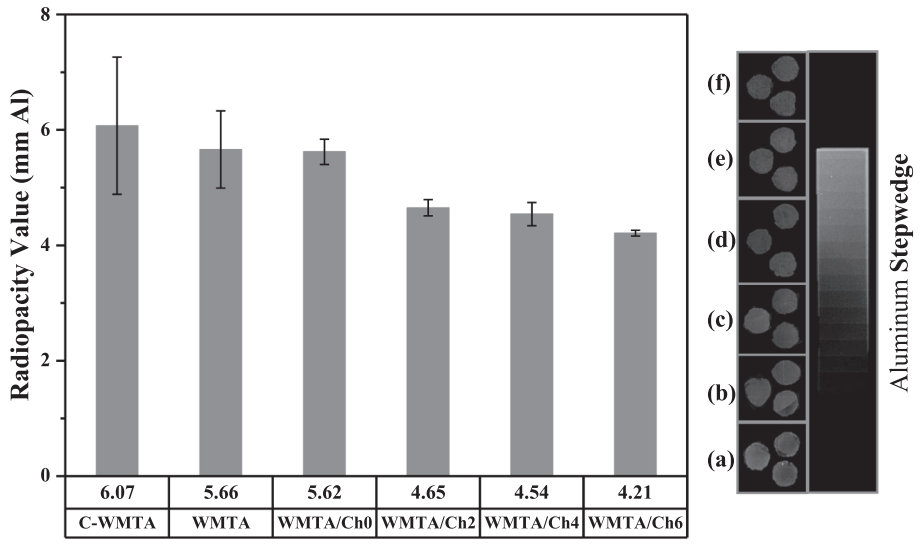


**Fig. 8.** The radiopacity of hydrated (a) C-WMTA, (b) WMTA, (c) WMTA/Ch0, (d) WMTA/Ch2, (e) WMTA/Ch4, and (f) WMTA/Ch6.

use of artificial saliva in investigating the mass loss of dental material is preferable compared to distilled water due to its similarity to creating a mimic biological environment.

The mass loss measurement on the first day of immersion is one of the critical factors in determining the effective and desirable endodontic WMTA regarding ANSI/ADA specification. The longer period measurement is conducted to substantiate the study of pH and $Ca^{2+}$ release. The mass fraction lost when WMTAs come into contact with artificial saliva solution is mainly composed of calcium hydroxide, yielding a high pH environment [22]. According to previous studies, most endodontic WMTA undergo the highest mass loss on the first immersion day. It indicates that the probability of microleakage formation in the dentin-material interface may occur and lead to bacterial colonization.

The subtraction of mass before and after immersion in artificial saliva solution of all tested groups is presented in Table 3. The mass loss test revealed that all agree with ISO 6876 that the acceptable mass loss of set WMTA is $\leq 3$ % by mass except for WMTA/Ch6, which undergoes 5.52 % mass loss after one day of immersion. The highest mass loss experienced by the WMTA/Ch6 is expected due to the low mechanical properties, explaining that the set cement is brittle and tends to be washed out quickly once immersed in the artificial saliva solution. In comparison, adding 4 wt% chitosan is assumed as the optimum composition for WMTA/Ch composite, which sustains the minor mass loss in all tested groups on day 1.

The observation of mass loss of WMTAs during the 7 days of immersion reveals that the mass loss decreases in all tested materials due to the more stable cement formation over time, except for WMTA/Ch4. The lower mass loss on day 7 is due to the formation of apatite crystals on the surface of the materials. This apatite formation is induced by the release of $Ca^{2+}$ ions contained in WMTAs. The apatite layer prevents further $Ca^{2+}$ release, avoiding mass loss increases [39]. The increase in mass loss of WMTA/Ch4 on day 7 indicates that the formation of the cement is not entirely stable. The set cement of WMTA generally reaches stability at 14 to 21 days after the hydration process, which means that there are no significant dimensional changes in the cement when exposed to a biological environment [25].

However, the optimum composition of WMTA:polymer will determine the composite material's properties [35]. The formation of hydrogen bonding via the intercalation mechanism occurs in the interface of the CSH interlayer. It will directly enhance the adhesion between aggregates in CSH cement, improve the mechanical properties, and reduce the mass loss of WMTA/chitosan composites.

The pH measurement aims to identify the alkaline properties of the soaking solution and the WMTA alkalization ability, which is utilized for antibacterial activity [25]. The pH data (Table 4) shows that the soaking solution of all tested groups is in an alkaline condition (pH $>$ 8) on the first day of immersion. The overall data reveals that a high pH level occurs after 1 day of immersion and decreases after 7 and 14 days due to the lower release of $Ca^{2+}$ in the cement material. It is suggested that the significant antibacterial activity lies on this point. When the WMTA is immersed in an artificial saliva solution, $Ca^{2+}$ ions are released and react with $OH^-$ further dissociating into $Ca^{2+}$ and $OH^-$, creating sterile surroundings. The highly alkaline environment can facilitate the penetration of $Ca^{2+}$ ions into the dentine tubules, which is clinically essential for cell mineralization [25,40]. The gradual decrease of pH value from day 1 to day 14 reveals the lessening of $Ca^{2+}$ ions released from the materials due to the formation of an apatite layer on the material's surface. The "mineral infiltration zone" at the dentin and WMTA contact is created when the environment is in high alkalinity conditions. It may cause dentinal collagen denaturation and helps $Ca^{2+}$ penetrate and exchange minerals [25]. The presence of chitosan in the WMTA is responsible for neutralizing the acidic environment through the protonation of its amino groups, enhancing the pH level of the soaking solution. Therefore, the quantity of corrosion, pore formation, and subsequent microleakage through those pores would be minimized since the acidity would be lower [36].

**Table 4**
Ph and $ca^{2+}$ ion release of tested groups in soaked solution.

| Sample Code | pH | | | $Ca^{2+}$ Ion Release (ppm) | | |
|---|---|---|---|---|---|---|
| | 1 Day | 7 Days | 14 Days | 1 Day | 7 Day | 14 Day |
| C-WMTA | 9.65 ± 0.47 | 8.66 ± 0.08 | 8.31 ± 0.00 | 105.84 ± 0.79 | 32.72 ± 0.00 | 31.90 ± 0.01 |
| WMTA | 8.44 ± 0.03 | 8.34 ± 0.01 | 7.85 ± 0.01 | 49.64 ± 0.19 | 26.73 ± 0.16 | 22.74 ± 0.41 |
| WMTA/ Ch0 | 8.39 ± 0.01 | 8.46 ± 0.03 | 8.34 ± 0.06 | 63.85 ± 0.38 | 29.25 ± 0.45 | 19.13 ± 0.74 |
| WMTA/ Ch2 | 8.46 ± 0.07 | 8.42 ± 0.01 | 7.88 ± 0.09 | 97.05 ± 0.74 | 28.31 ± 0.35 | 20.58 ± 0.37 |
| WMTA/ Ch4 | 8.51 ± 0.01 | 8.34 ± 0.06 | 7.97 ± 0.06 | 59.28 ± 0.49 | 25.99 ± 0.08 | 18.09 ± 0.00 |
| WMTA/ Ch6 | 8.39 ± 0.05 | 8.28 ± 0.07 | 8.10 ± 0.09 | 101.19 ± 0.58 | 30.05 ± 1.73 | 15.98 ± 0.00 |

The $Ca^{2+}$ ion release of all tested groups is measured after 1, 7, and 14 days of immersion in the artificial saliva solution. The data in Table 4. shows that the highest $Ca^{2+}$ ion release occurs on day 1 of all samples and tends to decrease over time which is appropriate to previous research. The decrease of $Ca^{2+}$ ion release happens over time due to the more stable cement formation [40]. The $PO_4^{2-}$ ions in artificial saliva solution react with the $Ca^{2+}$ ions to form calcium phosphate layers on the material's surface. The reaction of $Ca^{2+}$ and $PO_4^{2-}$ ions in the biological environment can induce the growth of the apatite layer. Hence the measurement of $Ca^{2+}$ ion release in this study may define the ability of dental material to activate mineralization [25]. The $Ca^{2+}$ ions release is a crucial factor in determining the biocompatibility of WMTAs. $Ca^{2+}$ ions may induce osteopontin regulation levels to increase dental pulp cells in the formation of the dentinal bridge [40]. The presence of chitosan in the WMTA composite is investigated to support the mineralization and formation of dentine through human periodontal ligament cells (HPLCs) [41]. This study shows the decreasing trends of $Ca^{2+}$ ion release, which defines that the WMTAs reach set cement.

The presence of chitosan in the CSH matrix can stabilize the amorphous calcium phosphate at the first stage of mineralization. The influence of the amino groups on the surface of chitosan in the physiological environment possesses a capacity to chelate $Ca^{2+}$ ions. The chelation further forms ionic clusters for regulating the mineral's nucleation and plays an essential role as a natural template for the growth of the apatite crystal [36]. Hence, the presence of chitosan may improve the biocompatibility of WMTAs.

### 3.2.4. *WMTA-Dentin interface evaluation*

Interaction between the dentinal wall and WMTA is one of the influencing factors in determining successful dental treatment. Dental materials must have the ability to interact with dental hard tissue resulting in a stable bonding of the WMTA-dentin interface. In this study, the evaluation of the WMTA-dentin interface was carried out by using SEM analysis (Fig. 9). The results reveal that C-WMTA and WMTA exhibit higher gaps between dentinal walls and WMTAs. In contrast, the cement composite with chitosan additives exhibits closer contact with the dentin surface. WMTA/Ch4 shows the most intimate contact with the dentinal wall by the gap of 1.4 μm. The closed contact of the WMTA/Ch-dentin interface is due to the biocompatibility and adhesive properties of chitosan, which may increase the adhesion stability of the WMTA-dentin interface. Hydroxyl and active amino groups in chitosan can be cross-linked with other reactive molecules in collagen fibers to form micro and nano fibrillar tissues within proteins hence providing a suitable sealing property [41]. The resulting gap value created by C-WMTA is consistent with the previous investigation [11]. The presence of chitosan may decrease the gap between dentin and WMTA, reducing microleakage formation. Furthermore, chitosan can deposit on the surface of the dentinal tubules resulting in more adhesion between the dentin and WMTA interface [36].

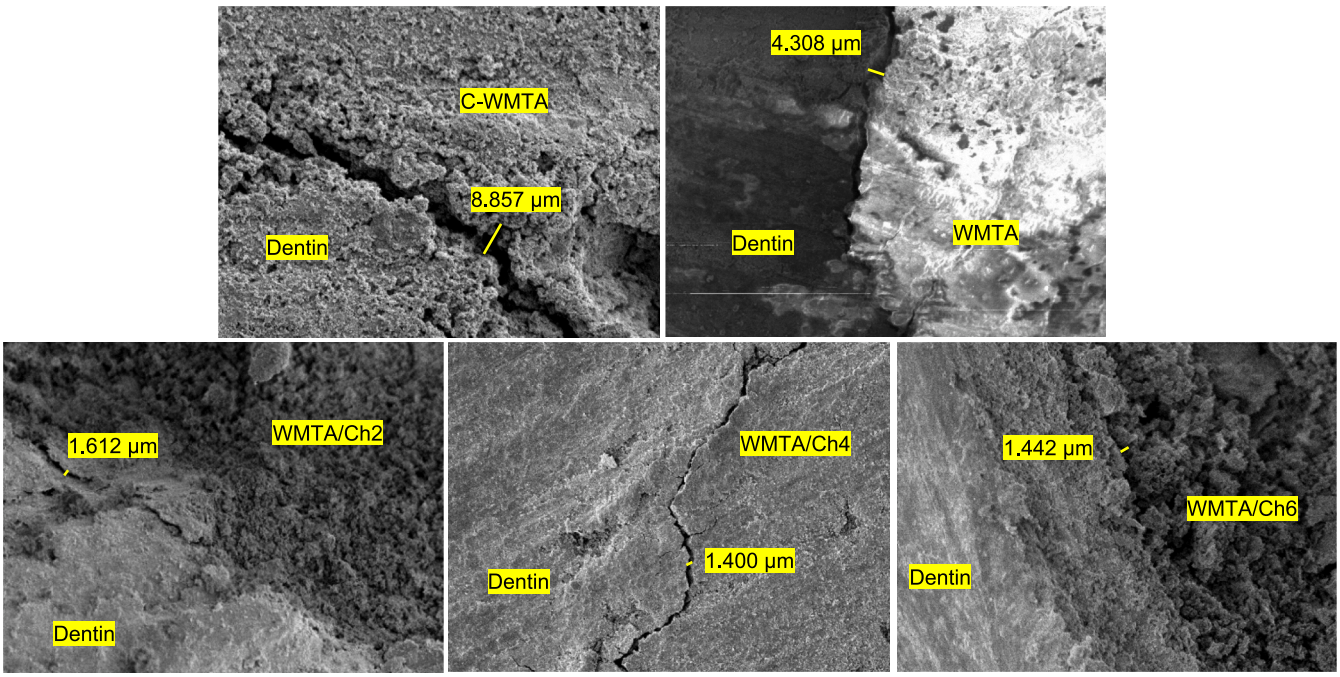


**Fig. 9.** SEM image showing the dentin – WMTA interface gap distance.

### 3.2.5. *Antibacterial activity*

In this experiment, the antibacterial activities of WMTA and WMTA/chitosan composites were determined by the disk diffusion method. The data presented in Table 5 shows that WMTA has the lowest level of antibacterial activity compared to other tested materials. The antibacterial property of WMTA is due to the sterile environment with high alkaline pH. The presence of Portlandite ($Ca(OH)_2$ in WMTA can be used as an intracanal medicament to eliminate remaining bacteria after endodontic treatment. The $OH^-$ ion may degrade the cytoplasmic membrane, structural proteins, and DNA of the bacteria, resulting in cell death [42] even though this effect is not sufficiently effective against *P. aeruginosa* and *E. faecalis*. It can be seen from the low value of the inhibition zone in WMTA.

WMTA/chitosan composites possess higher inhibition zones in both microorganisms than in WMTA. Besides the high pH level condition, the presence of amino groups in chitosan strongly affects the elimination of bacteria. The amino groups may assist in electrostatic interaction with the negative charge of the bacterial membrane, leading to intracellular leakage and death of cells [43]. In addition, the high pH level creates an alkaline condition, which facilitates biological activities on WMTAs [44]. However, there is no significant difference in inhibition zone value among the chitosan composites due to the slight range difference of chitosan concentration additives to WMTA. A previous study reveals that chitosan hybrid with calcium silicate enhanced the antibacterial activity of cement materials [42].

**Table 5**
Antibacterial activity of the tested groups.

| Samples | Inhibition Zone (mm) | |
|---|---|---|
| | *P. aeruginosa* | *E. faecalis* |
| Positive control | 23.6 ± 0.15 | 32.8 ± 0.25 |
| Negative control | 0.0 ± 0.00 | 0.0 ± 0.00 |
| WMTA | 5.0 ± 0.00 | 4.5 ± 0.71 |
| WMTA/Ch2 | 8.0 ± 1.42 | 9.0 ± 0.71 |
| WMTA/Ch4 | 8.5 ± 0.71 | 10.0 ± 0.00 |
| WMTA/Ch6 | 10.0 ± 0.00 | 10.0 ± 0.00 |

## 4. Conclusion

WMTA synthesized using the sol–gel method with temperature calcination of 1000 °C showed the presence of $C_3S$, $C_2S$, and $C_3A$ phases. The WMTA offers properties similar to C-WMTA. The hydrated WMTA modified with chitosan depicted the gel fiber of chitosan sticking in aggregates, and adding 2-4 wt% chitosan to WMTA improved its compressive strength and the diametral tensile strength. The percentage of weight loss and radiopacity results of the tested groups satisfied the requirement of standard dental material, except for WMTA modified with 6 wt%. Immersion of WMTAs in artificial saliva increase pH level towards alkaline condition by the release of $Ca^{2+}$ ion occurred in all tested groups, hence creating a sterile environment utilized for biological activity. The hydrated WMTA modified with 4 wt% showed the closest dentin-WMTA interface and antibacterial activity. From all the tests performed, it can be concluded that 4 wt% chitosan additive to WMTA is the appropriate composition to improve dental cement properties.

## Declaration of Competing Interest

The authors declare that they have no known competing financial interests or personal relationships that could have appeared to influence the work reported in this paper.

## Data availability

Data will be made available on request.

*Acknowledgments*

The first author thanks the Institut Teknologi Sumatera for the financial support of the research through the ITERA Scholarship Scheme.

*Data availability*

Data will be made available on request.

## References


[1] M. Kunert, M. Lukomska-Szymanska, Bio-inductive materials in direct and indirect pulp capping—A review article, Materials. 13 (2020) 1204, https://doi.org/10.3390/ma13051204.

[2] H.W. Choi, S. Um, S. Rhee, Synthesis of a $Ca_3SiO_5$ –$Ca_2SiO_4$ –$Ca_3Al_2O_6$ cement system with rapid setting capacity by spray-pyrolysis coupled with sol–gel method, J. Biomed. Mater. Res. 107 (2019) 1440–1451, https://doi.org/10.1002/jbm.b.34236.

[3] W.N. Ha, T. Nicholson, B. Kahler, L.J. Walsh, Mineral trioxide aggregate—A review of properties and testing methodologies, Materials. 10 (2017) 1261, https://doi.org/10.3390/ma10111261.

[4] G. Voicu, Sol-gel synthesis of white mineral trioxide aggregate with potential use as biocement, Rom. J. Mater. 7 (2012) 8.

[5] H.-J. Moon, J.-H. Lee, J.-H. Kim, J.C. Knowles, Y.-B. Cho, D.-H. Shin, H.-H. Lee, H.-W. Kim, Reformulated mineral trioxide aggregate components and the assessments for use as future dental regenerative cements, J Tissue Eng. 9 (2018) 204173141880739. 10.1177/2041731418807396.

[6] A.B.A. Hammad, A.M. Mansour, A.M.E. Nahrawy, $Ni^{2+}$ doping effect on potassium barium titanate nanoparticles: enhancement optical and dielectric properties, Physica Scripta. 96 (2021), 125821, https://doi.org/10.1088/1402-4896/ac25a6.

[7] S.M.M. Al-Hindawey, A.I. Ali, H.A. Zayed, A.M.E. Nahrawy, Magnetic topological insulators nano-crystallites $Fe_{1.4}Bi_{0.6}Se_{2.5}Y_{0.5}$Prx: Preparation, characterization and physical properties, ECS J. Solid State, Sci. Technol. 11 (2022), 053013, https://doi.org/10.1149/2162-8777/ac6f1e.

[8] M. Ghadafi, S.J. Santosa, Y. Kamiya, N. Nuryono, Free Na and less Fe compositions of $SiO_2$ extracted from rice husk ash as the silica source for synthesis of white mineral trioxide aggregate, KEM. 840 (2020) 311–317.

[9] A.M. El Nahrawy, B.A. Hemdan, A.M. Mansour, A. Elzwawy, A.B. Abou Hammad, Integrated use of nickel cobalt aluminoferrite/$Ni^{2+}$ nano-crystallites supported with $SiO_2$ for optomagnetic and biomedical applications, Mater. Sci. Eng. B. 274 (2021), 115491, https://doi.org/10.1016/j.mseb.2021.115491.

[10] D. Bokov, A. Turki Jalil, S. Chupradit, W. Suksatan, M. Javed Ansari, I.H. Shewael, G.H. Valiev, E. Kianfar, Nanomaterial by sol-gel method: Synthesis and application, Adv. Mater. Sci. Eng. 2021 (2021) 5102014, https://doi.org/10.1155/2021/5102014.

[11] F. Dewi, D. Asrianti, A. Margono, Microleakage evaluation of modified mineral trioxide aggregate effect toward marginal adaptation on cervical dentin perforation, Int J App Pharm. 9 (2018) 10. 10.22159/ijap.2017.v9s2.03.

[12] G. Pelliccioni, C. Vellani, M. Gatto, M. Gandolfi, C. Marchetti, C. Prati, Proroot mineral trioxide aggregate cement used as a retrograde filling without addition of water: An in vitro evaluation of its microleakage, J. Endod. 33 (2007) 1082–1085, https://doi.org/10.1016/j.joen.2007.04.009.

[13] I. Tsesis, S. Elbahary, N.B. Venezia, E. Rosen, Bacterial colonization in the apical part of extracted human teeth following root-end resection and filling: a confocal laser scanning microscopy study, Clin Oral Invest. 22 (2018) 267–274, https://doi.org/10.1007/s00784-017-2107-1.

[14] Y.-S. Noh, S.-H. Chung, K.S. Bae, S.-H. Baek, K.-Y. Kum, W.-C. Lee, W.-J. Shon, S.-H. Rhee, Mechanical properties and microstructure analysis of mineral trioxide aggregate mixed with hydrophilic synthetic polymer: Mineral trioxide aggregate mixed with PVA, J. Biomed. Mater. Res. 103 (2015) 777–782, https://doi.org/10.1002/jbm.b.33257.

[15] O. Duianat, A. Mahdian, N. Sanagoo, M.A. Mozayeni, S. Eskandarion, Setting time and surface microhardness of mineral trioxide aggregate and 1% and 5% fluoride-doped mineral trioxide aggregate mixed with water and gel-like polymer, Iran. Endod. J. 14 (2019). 10.22037/iej.v14i4.24094.

[16] A. Salem Milani, M. Froughreyhani, S. Charchi Aghdam, F. Pournaghiazar, M. Asghari Jafarabadi, Mixing with propylene glycol enhances the bond strength of mineral trioxide aggregate to dentin, J. Endod. 39 (2013) 1452–1455, https://doi.org/10.1016/j.joen.2013.05.005.

[17] Z. Aguilar, Harmouch, Hafdi, Bornert, Offner, Clauss, Fioretti, Huck, Benkirane-Jessel, Hua, Application of chitosan in bone and dental engineering, Molecules. 24 (2019) 3009, https://doi.org/10.3390/molecules24163009.

[18] D. Hu, Q. Ren, Z. Li, L. Zhang, Chitosan-based biomimetically mineralized composite materials in human hard tissue repair, Molecules. 25 (2020) 4785, https://doi.org/10.3390/molecules25204785.

[19] A. Zidan, Effect of chitosan on resin-dentin interface durability: A 2 year in-vitro study, Egypt. Dent. J. 65 (2019) 2955–2965. 10.21608/edj.2019.72691.

[20] H. Subhi, A. Husein, D. Mohamad, A.-A. Nurul, Physicochemical, mechanical and cytotoxicity evaluation of chitosan-based accelerated portland cement, J. Mater. Res. Technol. 9 (2020) 11574–11586, https://doi.org/10.1016/j.jmrt.2020.07.108.

[21] M. Fa'izzah, W. Widjijono, Y. Kamiya, N. Nuryono, Synthesis and characterization of white mineral trioxide aggregate using precipitated calcium carbonate extracted from limestone, KEM. 840 (2020) 330–335, https://doi.org/10.4028/www.scientific.net/KEM.840.330.

[22] W. Kurdowski, Portland cement clinker, in: cement and concrete chemistry, Springer Netherlands, Dordrecht, 2014: pp. 21–127. 10.1007/978-94-007-7945-7_2.

[23] N.C. Collier, Transition and decomposition temperatures of cement phases - a collection of thermal analysis data, Ceramics - Silikaty. (2016) 338–343. 10.13168/cs.2016.0050.

[24] M. Radwan, H. El-Hamid, S. Nagi, Synthesis, properties and hydration characteristics of novel nano-size mineral trioxide and tetracalcium phosphate for dental applications, Orient. J. Chem. 32 (2016) 2459–2472, https://doi.org/10.13005/ojc/320516.

[25] S. Kumari, A. Mittal, S. Dadu, A. Dhaundiyal, A. Abraham, B. Yendrembam, Comparative evaluation of physical and chemical properties of calcium silicate-based root-end filling materials (Mineral trioxide aggregate and biodentine): An *in vitro* study, Indian J Dent Sci. 10 (2018) 197, https://doi.org/10.4103/IJDS.IJDS_42_18.

[26] A. Bikharudin, S. Sutarno, Y. Kamiya, N. Nuryono, Effect of thermal treatment on physico-chemical properties of white mineral trioxide aggregate synthesized from limestone precipitate calcium carbonate, KEM. 884 (2021) 290–297, https://doi.org/10.4028/www.scientific.net/KEM.884.290.

[27] Faouzi.H. Maurice. Abou Rida, Synthesis and characterization of amorphous silica nanoparticles from aqueous silicates using cationic surfactants, Mater. Miner. 1. 24 (2014) 10.14456/JMMM.2014.7.

[28] M.E.-S. Ismaiel Saraya, H.H.A.E.-L. Rokbaa, formation and stabilization of vaterite calcium carbonate by using natural polysaccharide, ANP. 06 (2017) 158–182. 10.4236/anp.2017.64014.

[29] Q. Li, N.J. Coleman, The hydration chemistry of ProRoot MTA, Dent. Mater. J. 34 (2015) 458–465, https://doi.org/10.4012/dmj.2014-309.

[30] X. Ren, W. Zhang, J. Ye, FTIR study on the polymorphic structure of tricalcium silicate, Cem. Concr. Res. 99 (2017) 129–136, https://doi.org/10.1016/j.cemconres.2016.11.021.

[31] A.M. Abouelnaga, T.M. Meaz, A.M. Othman, R.A. Ghazy, A.M. El Nahrawy, Probing the structural and antimicrobial study on a sol–gel derived velosef-loaded bioactive calcium magneso-silicate xerogel, Silicon. 13 (2021) 623–631, https://doi.org/10.1007/s12633-020-00448-8.

[32] A.M. El Nahrawy, A.M. Mansour, A.B. Abou Hammad, R.S. Ibrahim, A. M. Abouelnaga, M.S. Abdel-Aziz, Optical, functional impact and antimicrobial of chitosan/phosphosilicate/$Al_2O_3$ nanosheets, J Inorg Organomet Polym. 30 (2020) 3084–3094, https://doi.org/10.1007/s10904-020-01469-x.

[33] A.M. El Nahrawy, A.S. Montaser, A.B. Abou Hammad, M. Ezzat, M. El-shakankery, Copper lithium silicate/$ZrO_2$ nanoparticles-coated Kevlar for improving UV-Vis absorbance/ protection properties, Silicon. 12 (2020) 1743–1750, https://doi.org/10.1007/s12633-019-00271-w.

[34] R. Grazziotin-Soares, M.H. Nekoofar, T.E. Davies, A. Bafail, E. Alhaddar, R. Hübler, A.L.S. Busato, P.M.H. Dummer, Effect of bismuth oxide on white mineral trioxide aggregate: chemical characterization and physical properties, Int Endod J. 47 (2014) 520–533, https://doi.org/10.1111/iej.12181.

[35] K. Yousefi, H.D. Manesh, A.R. Khalifeh, F. Moazami, M.R. Sanaee, Nanocement/poly(vinyl alcohol) composites for endodontic applications, Mater. Chem. Phys. 254 (2020), 123337, https://doi.org/10.1016/j.matchemphys.2020.123337.

[36] A. Kamali, S. Javadpour, B. Javid, N. Kianvash Rad, S. Naddaf Dezfuli, Effects of chitosan and zirconia on setting time, mechanical strength, and bioactivity of calcium silicate-based cement, Int J Appl Ceram Technol. 14 (2017) 135–144, https://doi.org/10.1111/ijac.12636.

[37] P. Wang, G. Qiao, Y. Zhang, D. Hou, J. Zhang, M. Wang, X. Wang, X. Hu, Molecular dynamics simulation study on interfacial shear strength between calcium-silicate-hydrate and polymer fibers, Constr. Build. Mater. 257 (2020), 119557, https://doi.org/10.1016/j.conbuildmat.2020.119557.

[38] D. Hou, J. Yu, P. Wang, Molecular dynamics modeling of the structure, dynamics, energetics and mechanical properties of cement-polymer nanocomposite, Compos. B. Eng. 162 (2019) 433–444, https://doi.org/10.1016/j.compositesb.2018.12.142.

[39] M. Kaup, E. Schäfer, T. Dammaschke, An in vitro study of different material properties of Biodentine compared to ProRoot MTA, Head Face Med. 11 (2015) 16, https://doi.org/10.1186/s13005-015-0074-9.

[40] S. Yamamoto, L. Han, Y. Noiri, T. Okiji, Evaluation of the Ca ion release, pH and surface apatite formation of a prototype tricalcium silicate cement, Int Endod J. 50 (2017) e73–e82, https://doi.org/10.1111/iej.12737.

[41] E. Ozlek, P.P. Rath, A. Kishen, P. Neelakantan, A chitosan-based irrigant improves the dislocation resistance of a mineral trioxide aggregate-resin hybrid root canal sealer, Clin Oral Invest. 24 (2020) 151–156, https://doi.org/10.1007/s00784-019-02916-x.

[42] M.-C. Lin, C.-C. Chen, I.-T. Wu, S.-J. Ding, Enhanced antibacterial activity of calcium silicate-based hybrid cements for bone repair, Mater. Sci. Eng. C. 110 (2020), 110727, https://doi.org/10.1016/j.msec.2020.110727.

[43] S. Abusrewil, J.L. Brown, C. Delaney, M.C. Butcher, M. Tiba, J.A. Scott, G. Ramage, W. McLean, Chitosan enhances the anti-biofilm activity of biodentine against an interkingdom biofilm model, Antibiotics. 10 (2021) 1317, https://doi.org/10.3390/antibiotics10111317.

[44] T. Prathita, N.K. Djauharie, R. Meidyawati, Antimicrobial activity of mineral trioxide aggregate and calcium hydroxide sealer on *Enterococcus faecalis* strain ATCC29212, Int J App Pharm. (2019) 123–125. 10.22159/ijap.2019.v11s1.AR178.